DNS of mass transfer in bi-dispersed bubble swarms *

Néstor Balcázar-Arciniega[1][0000−0003−0776−2086], Joaquim Rigola[1][0000−0002−6685−3677], and Assensi Oliva[1][0000−0002−2805−4794]

[1] Heat and Mass Transfer Technological Centre, Universitat Politècnica de Catalunya-BarcelonaTech. Colom 11, 08222, Terrassa (Barcelona), Spain
nestor.balcazar@upc.edu, nestorbalcazar@yahoo.es

Abstract. This work presents Direct Numerical Simulation of mass transfer in a bi-dispersed bubble swarm at high Reynolds number, by using a multiple marker level-set method. Transport equations are discretized by the finite-volume method on 3D collocated unstructured meshes. Interface capturing is performed by the unstructured conservative level-set method, whereas the multiple marker approach avoids the so-called numerical coalescence of bubbles. Pressure-velocity coupling is solved by the classical fractional-step projection method. Diffusive terms are discretized by a central difference scheme. Convective term of momentum equation, level-set equations, and mass transfer equation, are discretized by unstructured flux-limiters schemes. This approach improves the numerical stability of the unstructured multiphase solver in bubbly flows with high Reynolds number and high-density ratio. Finally, this numerical model is applied to research the effect of bubble-bubble interactions on the mass transfer in a bi-dispersed bubble swarm.

Keywords: Mass transfer · Bubbly flow · Unstructured flux-limiters · Unstructured meshes · Level-set method · Finite volume method · High-Performance Computing.

1 Introduction

Mas transfer in poly-dispersed bubble swarms is frequent in nature and industry. For instance, bubbly flows are employed in chemical reactors to produce chemical products, as well as to improve mass transfer rates in the so-called unit operations of chemical engineering. Although empirical correlations have been reported to estimate mass transfer rates in bubbles [18], the interplay between fluid mechanics and mass transfer in turbulent bi-dispersed bubble swarms is not well understood yet. Indeed, beyond the scientific motivation, understanding this phenomenon has practical importance in the design, optimization, and operation of industrial multiphase systems.

* Néstor Balcázar, as a Professor Serra-Húnter (UPC-LE8027), acknowledges the Catalan Government for the financial support through this programme. The authors acknowledges the financial support of the *Ministerio de Economía y Competitividad, Secretaría de Estado de Investigación, Desarrollo e Innovación* (MINECO), Spain (PID2020-115837RB-100). Simulations were executed using computing time granted by the RES (IM-2021-3-0013, IM-2021-2-0020, IM-2021-1-0013, IM-2020-2-0002, IM-2019-3-0015) on the supercomputer MareNostrum IV based in Barcelona, Spain.

ICCS Camera Ready Version 2022
To cite this paper please use the final published version:
DOI: 10.1007/978-3-031-08760-8_24

The development of supercomputers has promoted High-Performance computing (HPC) and Direct Numerical Simulation (DNS) of Navier-Stokes equations, as a pragmatic method to perform non-invasive numerical experiments of bubbly flows. In this sense, multiple numerical methods have been reported for DNS of two-phase flows, for instance: volume-of-fluid (VOF) methods [27], level-set (LS) methods [34,37], conservative level-set (CLS) methods [33,3], front tracking (FT) methods [41], and hybrid VOF/LS methods [38,39,6]. Some of these methods have been extended for interfacial heat transfer and mass transfer in gas-liquid multiphase flows, as reported in [22,15,2,16,21]. On the other hand, few works have been performed on DNS of mass transfer in bubble swarms [1,36,30,10,14,12]. Nevertheless, no previous studies of mass transfer in bi-dispersed bubble swarms have been reported in the context of the unstructured CLS method [10]. Therefore, this work aims to fill this lack in technical literature.

As advantages of present methodology, the unstructured CLS method [3,10] has been implemented on 3D collocated unstructured meshes, whereas the accumulation of mass conservation error inherent to standard level-set methods is circumvented. Furthermore, unstructured flux-limiters schemes as proposed in [3,7,10], are used to discretize the convective term of transport equations, avoiding numerical oscillations around discontinuities, and minimizing the so-called numerical diffusion [3,7,10]. Altogether, this numerical methods improve the numerical stability of the unstructured multiphase solver [3,4,5,6,7,10,14,12,13] in DNS of bubbly flows with high Reynolds number and high density ratio.

This paper is organized as follows: The mathematical model and numerical methods are presented in section 2. Numerical experiments are presented in section 3. Concluding remarks and future work are discussed in section 4.

2 Mathematical model and numerical methods

2.1 Incompressible two-phase flow

The one-fluid formulation [41], is employed to introduce surface tension force as a singular terms in Navier-Stokes equations:

$$\frac{\partial}{\partial t}(\rho \mathbf{v}) + \nabla \cdot (\rho \mathbf{v}\mathbf{v}) = -\nabla p + \nabla \cdot \mu \left(\nabla \mathbf{v}\right) + \nabla \cdot \mu (\nabla \mathbf{v})^T + (\rho - \rho_0)\mathbf{g} + \mathbf{f}_\sigma, \quad (1)$$

$$\nabla \cdot \mathbf{v} = 0, \quad (2)$$

where $\mathbf{v}$ is the fluid velocity, p denotes the pressure field, ρ is the fluid density, μ is the dynamic viscosity, $\mathbf{g}$ is the gravitational acceleration, $\mathbf{f}_\sigma$ is the surface tension force per unit volume concentrated at the interface, subscripts d and c denote the dispersed phase (bubbles or droplets) and continuous phase respectively. Density and viscosity are constant at each fluid-phase, whereas a jump discontinuity is present at the interface Γ:

$$\rho = \rho_d H_d + \rho_c H_c, \ \mu = \mu_d H_d + \mu_c H_c. \quad (3)$$

Here H_c is the Heaviside step function that is one at fluid c (Ω_c) and zero elsewhere, whereas $H_d = 1 - H_c$. At discretized level physical properties are regularized in order

ICCS Camera Ready Version 2022
To cite this paper please use the final published version:
DOI: 10.1007/978-3-031-08760-8_24

to avoid numerical instabilities around the interface. On the other hand, bi-dispersed bubble swarms are simulated in a full-periodic cubic domain ($y - axis$ aligned to $\mathbf{g}$), therefore a force $-\rho_0\mathbf{g}$ is included in momentum transport equation, Eq. (1), with $\rho_0 = V_\Omega^{-1}\int_\Omega (\rho_d H_d + \rho_c H_c)\, dV$, to avoid the acceleration of the entire flow field in the downward vertical direction [23,4,8,10],

2.2 Multiple marker unstructured CLS method and surface tension

The unstructured conservative level-set method (UCLS) [3,10] developed for interface capturing on unstructured meshes is employed in this research. Furthermore, to avoid the numerical coalescence of bubbles, each fluid particle (bubble or droplet) is represented by a level-set function, as proposed in [4,7,8,10]. Therefore, the interface of the ith fluid particle is defined as the 0.5 iso-surface of the level-set function ϕ_i, where $i = 1, 2, ..., n_d$ and n_d is the total number of fluid particles in Ω_d. Since incompressible flow is assumed (Eq. 2), the ith interface transport equation can be written in conservative form as follows:

$$\frac{\partial \phi_i}{\partial t} + \nabla \cdot \phi_i \mathbf{v} = 0,\ i = 1, .., n_d. \tag{4}$$

Furthermore, a re-initialization equation is introduced to keep a sharp and constant level-set profile on the interface:

$$\frac{\partial \phi_i}{\partial \tau} + \nabla \cdot \phi_i(1-\phi_i)\mathbf{n}_i^0 = \nabla \cdot \varepsilon \nabla \phi_i,\ i = 1, .., n_d. \tag{5}$$

where $\mathbf{n}_i^0$ denotes $\mathbf{n}_i$ evaluated at $\tau = 0$. Eq.(5) is advanced in pseudo-time τ up to achieve the steady state. The compressive term of Eq.(5), $\phi_i(1-\phi_i)\mathbf{n}_i^0$, forces the level-set function to be compressed onto the diffuse interface, along $\mathbf{n}_i$. The diffusive term, $\nabla \cdot \varepsilon \nabla \phi_i$, keeps the level-set profiles with characteristic thickness $\varepsilon = 0.5h^{0.9}$, where h is the local grid size [3,7,10]. Geometrical properties of the interface, such as normal vectors $\mathbf{n}_i$ and curvatures κ_i, are computed as follows:

$$\mathbf{n}_i(\phi_i) = \frac{\nabla \phi_i}{\|\nabla \phi_i\|},\ \kappa_i(\phi_i) = -\nabla \cdot \mathbf{n}_i,\ i = 1, .., n_d. \tag{6}$$

Surface tension forces are approximated by the Continuous Surface Force model [17], which has been extended to the multiple marker level-set method in [4,7,8,10]:

$$\mathbf{f}_\sigma = \sum_{i=1}^{n_d} \sigma \kappa_i(\phi_i)\mathbf{n}_i \delta_i^s = \sum_{i=1}^{n_d} \sigma \kappa_i(\phi_i) \nabla \phi_i. \tag{7}$$

where the regularized Dirac delta function is defined as $\delta_i = ||\nabla \phi||$ [3,4,7,8,10]. Finally, in order to avoid numerical instabilities at the interface, fluid properties in Eq. (3) are regularized by using a global level-set function ϕ [4,7], defined as follows:

$$\phi = min\{\phi_1, ..., \phi_{n_d}\}. \tag{8}$$

Thus, Heaviside functions presented in Eq.(3) are regularized as $H_d = 1 - \phi$ and $H_c = \phi$. In this work $0 < \phi \leq 0.5$ for Ω_d, and $0.5 < \phi \leq 1$ for Ω_c. Alternatively, if $0 < \phi \leq 0.5$ for Ω_c, and $0.5 < \phi \leq 1$ for Ω_d, then $H_d = \phi$ and $H_c = 1 - \phi$, whereas $\phi = max\{\phi_1, ..., \phi_{n_d}\}$ [10].

ICCS Camera Ready Version 2022
To cite this paper please use the final published version:
DOI: 10.1007/978-3-031-08760-8_24

2.3 Mass transfer

This work is focused in external mass transfer in bi-dispersed bubble swarms. Therefore, the concentration of chemical species in the continuous phase is computed by a convection-diffusion-reaction equation, as follows [10]:

$$\frac{\partial C}{\partial t} + \nabla \cdot (\mathbf{v}C) = \nabla \cdot (\mathcal{D}\nabla C) + \dot{r}(C), \tag{9}$$

where C denotes the chemical species concentration field, $\mathcal{D}$ denotes the diffusion coefficient or diffusivity which is equal to $\mathcal{D}_c$ in Ω_c and $\mathcal{D}_d$ elsewhere, $\dot{r}(C) = -k_1 C$ is the overall chemical reaction rate, k_1 is the first-order reaction rate constant. Furthermore, the concentration inside the bubbles is kept constant [21,36,1,10], whereas convection, diffusion and reaction of the mass dissolved from Ω_d exists only in Ω_c.

As proposed in [10], linear interpolation is applied to compute the concentration (C_P) at the interface cells, taking information from Ω_c (excluding interface cells), and imposing a Dirichlet boundary condition for the concentration at the interface ($\phi = 0.5$). Further details are reported in [10].

2.4 Numerical methods

Transport equations are discretized by the finite-volume method on 3D collocated unstructured meshes, as introduced in [3,7,10]. For the sake of completeness, some points are remarked in what follows.

The convective term of momentum equation (Eq. (1)), level-set advection equation (Eq. (4)), and transport equation for concentration of chemical species (Eq. (9)), is explicitly computed, by approximating the fluxes at cell faces with unstructured flux-limiter schemes, as first proposed in [3,10]. As a consequence, approximation of convective term is written in the current cell Ω_P as follows: $(\nabla_h \cdot \beta\psi\mathbf{v})_P = \frac{1}{V_P}\sum_f \beta_f \psi_f \mathbf{v}_f \cdot \mathbf{A}_f$, where V_P is the volume of the current cell Ω_P, subindex f denotes the cell-faces, $\mathbf{A}_f = ||\mathbf{A}_f||\mathbf{e}_f$ is the area vector, $\mathbf{e}_f$ is a unit-vector perpendicular to the face f pointing outside the cell Ω_P [3,10]. Here, $\beta_f = \{\rho_f, 1, 1\}$, consistently with Eqs.(1, 4, 9), is approximated by linear interpolation. An especial interpolation is applied to $(\mathbf{v}_f \cdot \mathbf{A}_f)$ [6], to avoid the pressure-velocity decoupling on collocated meshes. Finally, $\psi_f = \{\mathbf{v}_f, C_f, \phi_f\}$ is computed as the sum of a diffusive upwind part (ψ_{C_p}) plus an anti-diffusive term [3,7,10]:

$$\psi_f = \psi_{C_p} + \frac{1}{2} L(\theta_f)(\psi_{D_p} - \psi_{C_p}). \tag{10}$$

where $L(\theta_f)$ is the flux limiter, $\theta_f = (\psi_{C_p} - \psi_{U_p})/(\psi_{D_p} - \psi_{C_p})$, C_p is the upwind point, U_p is the far-upwind point, and D_p is the downwind point [10]. Some of the flux-limiters ($L(\theta)$)) implemented in the unstructured multiphase solver [3,4,5,6,7,8,10],

ICCS Camera Ready Version 2022
To cite this paper please use the final published version:
DOI: 10.1007/978-3-031-08760-8_24

have the form [40,24]:

$$L(\theta_f) \equiv \begin{cases} \max\{0, \min\{2\theta_f, 1\}, \min\{2, \theta_f\}\} & \text{superbee,} \\ (\theta_f + |\theta_f|)/(1 + |\theta_f|) & \text{van Leer,} \\ \max\{0, \min\{4\theta_f, 0.75 + 0.25\theta_f, 2\}\} & \text{smart,} \\ 1 & \text{CD,} \\ 0 & \text{Upwind.} \end{cases} \tag{11}$$

An assessment of flux-limiters to discretize the convective term of transport equations on unstructured meshes is presented in [10]. In this research, Superbee flux-limiter is employed unless otherwise stated. From the flux-limiters remarked in Eq.(11), SUPERBEE, VAN-LEER, SMART and UPWIND preserve the numerical stability of the multiphase solver, as these schemes avoid numerical oscillations around discontinuities. Concerning the called numerical diffusion, the SUPERBEE flux-limiter is the less diffusive scheme, whereas the UPWIND scheme maximizes the numerical diffusion. Thus, the selection of the SUPERBEE flux-limiter scheme is crucial for bubbly flows with high Reynolds number and high-density ratio, preserving numerical stability and minimizing the numerical diffusion.

Compressive term of the re-initialization equation (Eq. (5)), is discretized at the cell Ω_P as follows [10]: $(\nabla \cdot \phi_i(1-\phi_i)\mathbf{n}_i^0)_P = \frac{1}{V_P}\sum_f (\phi_i(1-\phi_i))_f \mathbf{n}_{i,f}^0 \cdot \mathbf{A}_f$, where $\mathbf{n}_{i,f}^0$ and $(\phi_i(1-\phi_i))_f$ are linearly interpolated. The diffusive term of transport equations are centrally differenced [10]. Linear interpolation is used to find the cell-face values of physical properties and interface normals unless otherwise stated. Gradients are computed at cell centroids through the least-squares method using the information of the neighbor cells around the vertexes of the current cell (see Fig. 2 of [3]). For instance at the cell Ω_P, the gradient of the variable $\psi = \{v_j, C, \phi, ...\}$ is calculated as follows:

$$(\nabla\psi)_P = (\mathbf{M}_P^T \mathbf{W}_P \mathbf{M}_P)^{-1} \mathbf{M}_P^T \mathbf{W}_P \mathbf{Y}_P, \tag{12}$$

$\mathbf{M}_P$ and $\mathbf{Y}_P$ are defined as introduced in [3], $\mathbf{W}_P = \text{diag}(w_{P\to1}, .., w_{P\to n})$ is the weighting matrix [29,32], defined as the diagonal matrix with elements $w_{P\to k} = \{1, ||\mathbf{x}_P - \mathbf{x}_k||^{-1}\}$, $k = \{1, .., n\}$, and subindex n is the number of neighbor cells. The impact of the selected weighting coefficient ($w_{P\to k}$) on the simulations is reported in our previous work [14].

The fractional-step projection method [19] is used to compute the pressure-velocity coupling. First, a predictor velocity ($\mathbf{v}_P^*$) is calculated at cell-centroids:

$$\frac{\rho_P \mathbf{v}_P^* - \rho_P^0 \mathbf{v}_P^0}{\Delta t} = \mathbf{C}_{\mathbf{v},P}^0 + \mathbf{D}_{\mathbf{v},P}^0 + (\rho_P - \rho_0)\mathbf{g} + \mathbf{f}_{\sigma,P}, \tag{13}$$

where the super-index 0 denotes the previous time-step, subindex P denotes the control volume Ω_P, $\mathbf{D}_\mathbf{v} = \nabla \cdot \mu\nabla\mathbf{v} + \nabla \cdot \mu(\nabla\mathbf{v})^T$, and $\mathbf{C}_\mathbf{v} = -\nabla \cdot (\rho\mathbf{v}\mathbf{v})$. Imposing the incompressibility constraint, $(\nabla \cdot \mathbf{v})_P = 0$, to the corrector step, Eq. (15), leads to a Poisson equation for the pressure at cell-centroids:

$$\left(\nabla \cdot \left(\frac{\Delta t}{\rho}\nabla p\right)\right)_P = (\nabla \cdot \mathbf{v}^*)_P\,, \ \mathbf{e}_{\partial\Omega} \cdot \nabla p|_{\partial\Omega} = 0. \tag{14}$$

ICCS Camera Ready Version 2022
To cite this paper please use the final published version:
DOI: 10.1007/978-3-031-08760-8_24

which is solved by means of a preconditioned conjugate gradient method. A Jacobi pre-conditioner is used in this research. Here $\partial\Omega$ denotes the boundary of Ω, excluding regions with periodic boundary condition, where information of the corresponding periodic nodes is used [10,4]. In a further step the updated velocity ($\mathbf{v}_P$) is computed at cell-centroids:

$$\frac{\rho_P \mathbf{v}_P - \rho_P \mathbf{v}_P^*}{\Delta t} = -(\nabla p)_P. \tag{15}$$

Furthermore, face-cell velocity $\mathbf{v}_f$ is interpolated [7,10] to fulfill the incompressibility constraint and to avoid pressure-velocity decoupling on collocated meshes [35]. Then, $\mathbf{v}_f$ or some equivalent variable (e.g., $\mathbf{v}_f \cdot \mathbf{A}_f$) is employed to advect $\beta_f \psi_f$ on the convective term of transport equations [7,10]. This approach benefits the numerical stability of the multiphase solver [3,4,5,6,7,8,10], specially for bubbly flows with high density ratio and high Reynolds numbers, as demonstrated in our previous works [4,8].

Temporal discretization of advection equation (Eq. (4)) and re-initialization equation (Eq. (5)) is performed by a TVD Runge-Kutta method [25]. Reinitialization equation (Eq. (5)), is solved for the steady state, using two iterations per physical time step to maintain the profile of the CLS functions [3,6,10].

The reader is referred to [3,4,5,7,8,10,14,13] for further technical details on the finite-volume discretization of transport equations on collocated unstructured grids. Numerical methods are implemented in the framework of the parallel C++/MPI code TermoFluids [10]. The parallel scalability of the multiple marker level-set solver is reported in [8,10].

3 Numerical experiments

Bubbles regimes can be characterized by the following dimensionless numbers [18]:

$$\begin{gathered} Mo = \frac{g\mu_c^4 \Delta\rho}{\rho_c^2 \sigma^3}, \quad Eo = \frac{g d^2 \Delta\rho}{\sigma}, \quad Re_i = \frac{\rho_c U_{Ti} d}{\mu_c}, \\ \eta_\rho = \frac{\rho_c}{\rho_d}, \quad \eta_\mu = \frac{\mu_c}{\mu_d}, \quad \alpha = \frac{V_d}{V_\Omega}, \quad \eta_d = \frac{d_b}{d_{b^*}}, \end{gathered} \tag{16}$$

where Mo is the Morton number, Eo is the Eötvös number, Re is the Reynolds number, η_ρ is the density ratio, η_μ is the viscosity ratio, $\Delta\rho = |\rho_c - \rho_d|$ is the density difference between the fluid phases, subscript d denotes the dispersed fluid phase, subscript c denotes the continuous fluid phase, Since a bi-dispersed bubble swarm will be simulated, η_d denotes the ratio of bubble diameters, d_b is the diameter of bigger bubbles, d_{b^*} is the diameter of smaller bubbles, $d = d_b$ will be taken as the characteristic bubble diameter employed to define $\{Mo, Eo, Re, Da, Pe, t^*\}$, α is the bubble volume fraction, V_d is the volume of bubbles (Ω_d), V_Ω is the volume of Ω, and $t^* = t\sqrt{g/d}$ is the dimensionless time.

Numerical results will be reported in terms of the so-called drift velocity [23,10], $U_{Ti}(t) = (\mathbf{v}_i(t) - \mathbf{v}_\Omega(t)) \cdot \hat{\mathbf{e}}_y$, which can be interpreted as the bubble velocity with respect to a stationary container, $\mathbf{v}_i(t)$ is the velocity of the ith bubble, $\mathbf{v}_\Omega(t)$ is the spatial averaged velocity in Ω.

ICCS Camera Ready Version 2022
To cite this paper please use the final published version:
DOI: 10.1007/978-3-031-08760-8_24

Mass transfer with chemical reaction, $\dot{r}(C) = -k_1 C$, is characterized by the Sherwood number (Sh), the Damköler (Da) number, and Schmidt number (Sc) or Peclet number (Pe), defined in Ω_c as follows:

$$Sh = \frac{k_c d}{\mathcal{D}_c},\ Sc = \frac{\mu_c}{\rho_c \mathcal{D}_c},\ Pe = \frac{U_T d}{\mathcal{D}_c} = ReSc,\ Da = \frac{k_1 d^2}{\mathcal{D}_c}. \tag{17}$$

where k_c is the mass transfer coefficient in Ω_c.

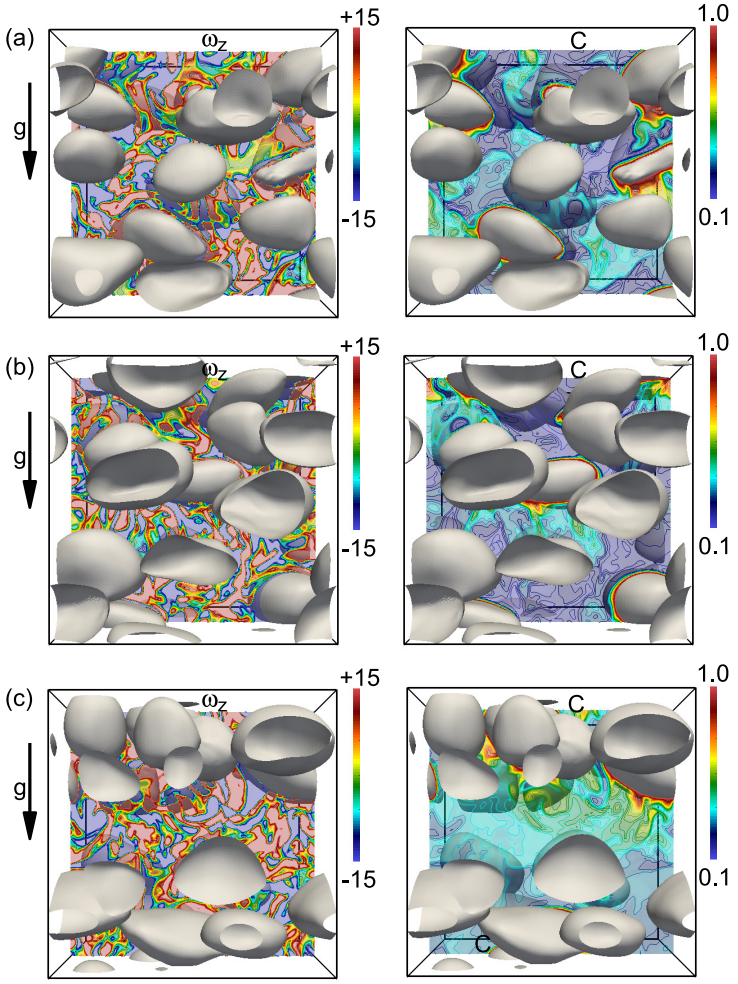

Fig. 1. Mass transfer in a bi-dispersed bubble swarm, $N_b = 16$ (total number of bubbles), in a full-periodic cube, $Eo = 4.0$, $d_b/d_{b^*} = 1.26$, $Mo = 5 \times 10^{-11}$, $\eta_\rho = \eta_\mu = 100$, $Sc = 1$, $Da = 170.7$, $\alpha = 19.6\%$, $\alpha_b = 13.1\%$, $\alpha_{b^*} = 6.54\%$. Vorticity ($\omega_z = \mathbf{e}_z \cdot \nabla \times \mathbf{v}$) and concentration ($C$) on the plane $x - y$ at (a) $t^* = tg^{1/2}d^{-1/2} = 7$, (b) $t^* = 14$, (c) $t^* = 21$.

ICCS Camera Ready Version 2022
To cite this paper please use the final published version:
DOI: 10.1007/978-3-031-08760-8_24

3.1 Validations and verifications

Multiple validations, verifications and extensions of the unstructured multiphase solver [3,10] are reported in our previous works, for instance: buoyancy-driven motion of single bubbles on unconfined domains [3,5,6], binary droplet collision with bouncing outcome [4], drop collision against a fluid interface without coalescence [4], bubbly flows in vertical channels [8,11], falling droplets [9], Taylor bubbles [26], thermocapillary-driven motion of deformable droplets [6], and liquid-vapor phase change [13]. A comparison of the unstructured CLS method [3] and coupled volume-of-fluid/level-set method [6] is reported in [9].

Concerning the mass transfer in single bubbles and mono-dispersed bubble swarms, on unconfined and confined domains, the reader is referred to our previous works [10,14,12], for validations and verifications of the multiple marker level-set solver employed in this research. Indeed, this work can be considered as a further step to perform Direct Numerical Simulation of mass transfer in bi-dispersed bubble swarms.

3.2 Mass transfer in a bi-dispersed bubble swarm

As a further step and with the confidence that the multiple marker level set solver has been validated [10,14,12,13], the DNS of mass transfer in a bi-dispersed bubble swarm is computed. The saturation of concentration of chemical species in Ω_c is avoided by the chemical reaction term in Eq.(9) [36,10]. Furthermore, a mass balance of the chemical species at steady state ($dC_c/dt = 0$) is employed to obtain the mass transfer coefficient (k_c) in Ω_c, as follows [10,12,14]:

$$k_c = \frac{V_c k_1 C_c}{(C_{\Gamma,c} - C_c)\sum_{i=1}^{n_d} A_i}. \tag{18}$$

Here $A_i = \int_\Omega \delta_i^s dV$ is the surface of the ith bubble, $C_c = V_c^{-1}\int_{\Omega_c} C dV$, and $\delta_i^s = ||\nabla\phi_i||$. Ω is a full-periodic cubic domain, with side length $L_\Omega = 3.18d$. Ω is discretized by 200^3 hexahedral control volumes, with grid size $h = L_\Omega/200$, distributed on 528 CPU-cores. As a consequence, bubbles are resolved with a grid size $h = d_b/63 = d_{b^*}/50$. In our previous works [10,14,12], it has been demonstrated that $h = d/35$ is enough to capture the hydrodynamics and mass transfer in gravity-driven bubbly flows [10]. Periodic boundary conditions are used on the $x-z$, $x-y$ and $y-z$ boundary planes. Bubbles are initially distributed in Ω following a random pattern, whereas fluids are quiescent. Since fluids are incompressible and bubble coalescence is not allowed, the void fraction ($\alpha = V_d/V_\Omega$) and number of bubbles are constant throughout the simulation.

Dimensionless parameters are $Eo = 4.0$, $d_b/d_{b^*} = 1.26$, $Mo = 5\times10^{-11}$, $\eta_\rho = \eta_\mu = 100$, $Sc = 1$, $Da = 170.7$, $\alpha = 19.6\%$, $\alpha_b = 13.1\%$, $\alpha_{b^*} = 6.54\%$, which corresponds to a bubbly flow with 16 bubbles distributed in Ω, 8 bubbles of diameter d_b and 8 bubbles of diameter d_b^*. Here α_b denotes the volume fraction of bigger bubbles, and α_{b^*} is the volume fraction of smaller bubbles. Fig. 1 illustrates the mass transfer from a bi-dispersed swarm of 16 bubbles at $t^* = \{7, 14, 21\}$. Furthermore, concentration contours (C), and vorticity contours ($\omega_z = \hat{\mathbf{e}}_z \cdot \nabla \times \mathbf{v}$) are

ICCS Camera Ready Version 2022
To cite this paper please use the final published version:
DOI: 10.1007/978-3-031-08760-8_24

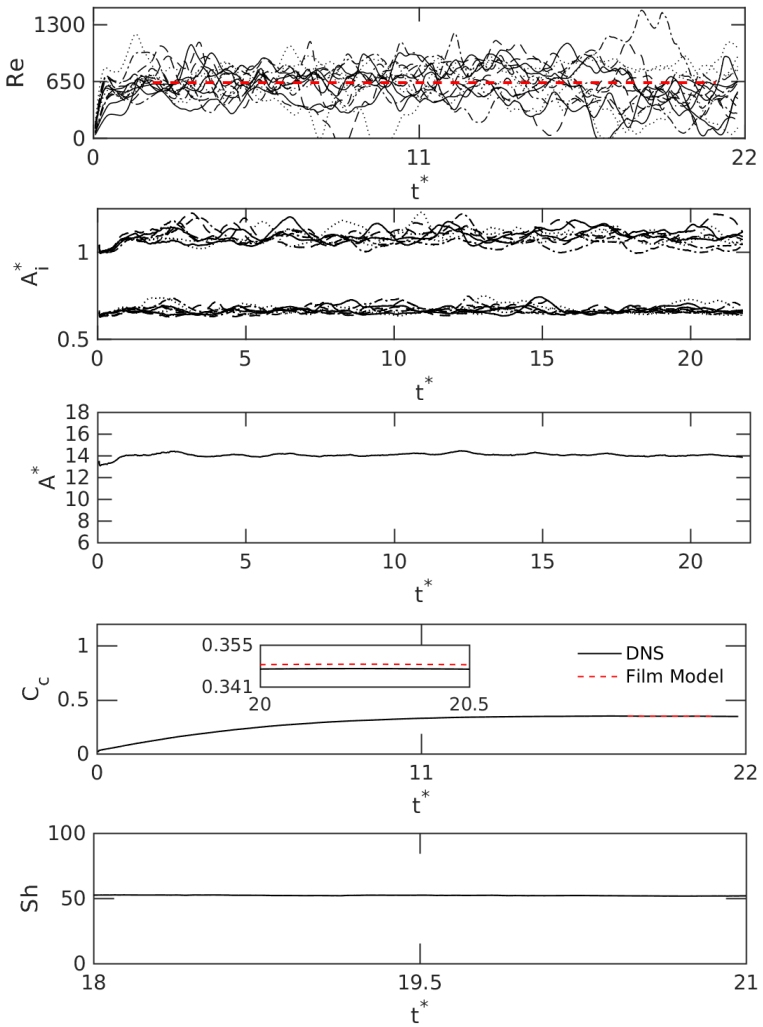

Fig. 2. Mass transfer from a bubble swarm, $N_b = 16$, in a full-periodic cube, $Eo = 4.0$, $d_b/d_{b^*} = 1.26$, $Mo = 5 \times 10^{-11}$, $\eta_\rho = \eta_\mu = 100$, $Sc = 1$, $Da = 170.7$, $\alpha = 19.6\%$, $\alpha_b = 13.1\%$, $\alpha_{b^*} = 6.54\%$. Time evolution of Reynolds number (Re) for each bubble (black lines), averaged Reynolds number for each bubble (continuous lines), time-averaged Reynolds number (red discontinuous line), normalized bubble surface $A_i^*(t)$, total interfacial surface of bubbles $A^*(t) = \sum_{i=1}^{n_d} A_i^*(t)$, spatial averaged concentration $C_c = V_c^{-1} \int_{\Omega_c} C dV$, and Sherwood number $Sh(t)$.

shown on the plane $x - y$. Fig. 2 shows the time evolution of Reynolds number for each bubble and the time-averaged Reynolds number (discontinuous red line), normalized surface of each bubble $A_i^*(t) = A_i(t)/(4\pi d_b^2)$, total normalized surface of bubbles

ICCS Camera Ready Version 2022
To cite this paper please use the final published version:
DOI: 10.1007/978-3-031-08760-8_24

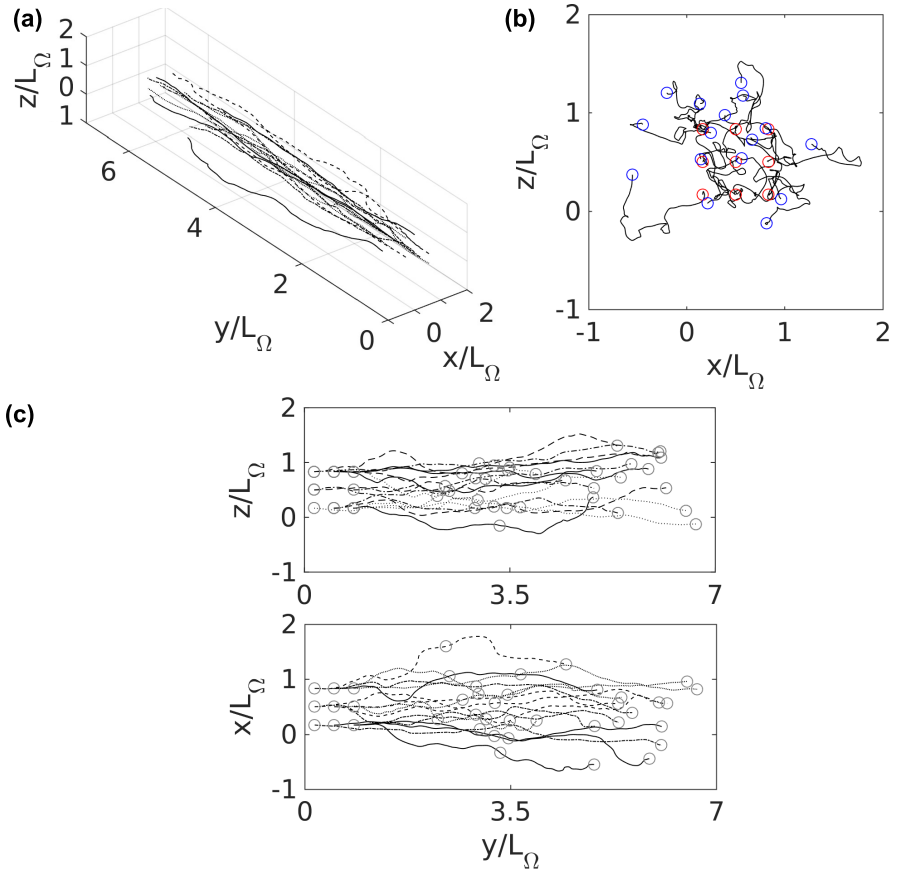

Fig. 3. Mass transfer from a bubble swarm, $N_b = 16$, in a full-periodic cube, $Eo = 4.0$, $d_b/d_{b^*} = 1.26$, $Mo = 5 \times 10^{-11}$, $\eta_\rho = \eta_\mu = 100$, $Sc = 1$, $Da = 170.7$, $\alpha = 19.6\%$, $\alpha_b = 13.1\%$, $\alpha_{b^*} = 6.54\%$. (a) 3D bubble trajectories. (b) Projection of bubble trajectories on the plane $x - z$. (c) Projection of bubble trajectories on the plane $x - y$ and $z - y$. Here L_Ω is the side-length of the periodic cubic domain.

$A^*(t) = \sum_{i=1}^{n_d} A_i^*(t)$, space-averaged concentration of chemical species (C_c) in Ω_c, and Sherwood number $Sh(t)$ at steady state ($dCc/dt = 0$). Strong deformation of bubble shapes ($A_i^*(t)$), bubble-bubble interactions, and path instabilities of bubbles at high Reynolds numbers, lead to fluctuations in $Re_i(t)$ as illustrated in Fig. 2. On the other hand, the Reynold number of the bi-dispersed bubble swarm, $\bar{Re} = n_d^{-1} \sum_{i=1}^{n_d} Re_i(t)$, tends to the steady-state. The spatial averaged concentration (C_c) achieves an steady-state value after initial transient effects, which demonstrates an equilibrium between mass transfer from the bubbles to Ω_c and the chemical reaction in Ω_c. As a consistency test, numerical results of the space-averaged concentration of chemical species in Ω_c compares very well with results obtained by the called film theory [10], as illustrated

ICCS Camera Ready Version 2022
To cite this paper please use the final published version:
DOI: 10.1007/978-3-031-08760-8_24

in Fig. 2. Furthermore, the mass transfer coefficient ($Sh \approx 50$) achieves the steady-state, once $dC_c/dt = 0$. Finally, Fig. 3 illustrates bubble trajectories, which indicate a repulsion effect between the bubbles.

4 Conclusions

DNS of mass transfer in a bi-dispersed bubble swarm has been performed using a parallel multiple-marker level-set method [4,8,10]. Numerical experiments demonstrate the reliability of this approach as an accurate tool for simulating bi-dispersed bubbly flows with mass transfer and chemical reaction in a full-periodic domain. The solver can reproduce the physics of bubble-bubble interactions in a long-time simulation of bubbly flows. This numerical approach avoids the numerical merging of bubbles, an artifact inherent to interface capturing methods, e.g., level-set, volume-of-fluid. Bubble-bubble interactions lead to a repulsion effect in horizontal alignment. On the other hand, when two bubbles are vertically aligned, their interactions follow the so-called drafting-kissing-tumbling mechanism observed in solid particles. This set of interactions induces a fluctuating velocity field known in the literature as bubble-induced turbulence. The time-averaged Reynolds number (Re) and Sherwood number (Sh) tend to the steady-state. Turbulence induced by the agitation of bubbles promotes the mixing of chemical species in the continuous phase. Furthermore, the spatially averaged concentration of chemical species tends to the steady-state, indicating a balance between chemical reaction in Ω_c and mass transfer from bubbles. Present results demonstrate that the multiple marker level-set method [10] is a predictive model to compute $Sh = Sh(Eo, Re, Da, \alpha_b\alpha_{b^*}, d_b/d_{b^*})$ in bi-dispersed bubbly flows. In future work, the model will be extended to simulate complex chemical reaction kinetics, as well as employed in parametric studies of $Sh = Sh(Eo, Re, Da, ...)$ to develop closure relations for models based on the averaged flow, e.g., two-fluid models [28].

References

1. Aboulhasanzadeh, B., Thomas, S., Taeibi-Rahni, M., Tryggvason, G. (2012). Multiscale computations of mass transfer from buoyant bubbles. *Chemical Engineering Science* 75, 456-467.
2. Alke, A., Bothe, D., Kroeger, M., Warnecke, H.J. (2009). VOF-based simulation of conjugate mass transfer from freely moving fluid particles. In Mammoli, AA and Brebbia, CA (Ed): *Computational methods in multiphase flow V, WIT Transactions on Engineering Sciences*, 157-168.
3. Balcázar, N., Jofre, L., Lehmkhul, O., Castro, J., Rigola, J. (2014). A finite-volume/level-set method for simulating two-phase flows on unstructured grids. *International Journal of Multiphase Flow* 64, 55-72
4. Balcázar, N., Lehmkhul, O., Rigola, J., Oliva, A. (2015). A multiple marker level-set method for simulation of deformable fluid particles. *International Journal of Multiphase Flow* 74, 125-142
5. Balcázar, N., Lemhkuhl, O., Jofre, L., Oliva, A. (2015). Level-set simulations of buoyancy-driven motion of single and multiple bubbles. *International Journal of Heat and Fluid Flow* 56, 91-107

ICCS Camera Ready Version 2022
To cite this paper please use the final published version:
DOI: 10.1007/978-3-031-08760-8_24

6. Balcázar, N., Lehmkhul, O., Jofre, L., Rigola, J., Oliva, A. (2016). A coupled volume-of-fluid/level-set method for simulation of two-phase flows on unstructured meshes. *Computers and Fluids* 124, 12-29.
7. Balcázar, N., Rigola, J., Castro, J., Oliva, A. (2016). A level-set model for thermocapillary motion of deformable fluid particles. *International Journal of Heat and Fluid Flow* 62, Part B, 324-343.
8. Balcázar, N., Castro, J., Rigola, J., Oliva, A. (2017). DNS of the wall effect on the motion of bubble swarms. *Procedia Computer Science* 108, 2008-2017.
9. Balcázar, N., Castro, J., Chiva, J., Oliva, A. (2018). DNS of Falling Droplets in a Vertical Channel. *International Journal of Computational Methods and Experimental Measurements*, Volume 6 (2018), Issue 2., 398-410.
10. Balcázar, N., Antepara, O., Rigola, J., Oliva, A. (2019) A level-set model for mass transfer in bubbly flows. *International Journal of Heat and Mass Transfer*. (Accepted, 2 Apr 2019)
11. Balcázar N., Lehmkuhl O., Castro J., Oliva A. (2018). DNS of the Rising Motion of a Swarm of Bubbles in a Confined Vertical Channel. In: Grigoriadis D., Geurts B., Kuerten H., Frhlich J., Armenio V. (eds) *Direct and Large-Eddy Simulation X. ERCOFTAC Series*, vol 24. Springer, Cham.
12. Balcázar N., Antepara O., Rigola J., Oliva A. (2020). DNS of Drag-Force and Reactive Mass Transfer in Gravity-Driven Bubbly Flows. In: Garca-Villalba M., Kuerten H., Salvetti M. (eds) *Direct and Large Eddy Simulation XII. DLES 2019. ERCOFTAC Series*, vol 27. Springer, Cham.
13. N. Balcazar, J. Rigola and A. Oliva, (2021). Unstructured Level-Set Method For Saturated Liquid-Vapor Phase Change, in: WCCM-ECCOMAS2020. URL `https://www.scipedia.com/public/Balcazar_et_al_2021a`, doi: 10.23967/wccm-eccomas.2020.352
14. Balcázar-Arciniega N., Rigola J., Oliva A. (2019) DNS of Mass Transfer from Bubbles Rising in a Vertical Channel. In: *Rodrigues J. et al. (eds) Computational Science ICCS 2019. ICCS 2019. Lecture Notes in Computer Science*, vol 11539. Springer, Cham
15. Bothe, D., Koebe, M., Wielage, K., Warnecke, H.J. (2003). VOF simulations of mass transfer from single bubbles and bubble chains rising in the aqueous solutions, In Proceedings of FEDSM03: *Fourth ASME-JSME Joint Fluids Engineering Conference*, Honolulu, HI, USA, July 611.
16. Bothe, D., Fleckenstein, S. (2013). Modeling and VOF-based numerical simulation of mass transfer processes at fluidic particles. *Chem. Eng. Science* 101, 283-302.
17. Brackbill, J.U., Kothe, D.B., Zemach, C. (1992). A Continuum Method for Modeling Surface Tension, *J. Comput. Phys.* 100, 335-354.
18. Clift, R., Grace, J.R., Weber, M.E. Bubbles, Drops and Particles. Academin Press, New York, 1978.
19. Chorin, A.J. (1968). Numerical solution of the Navier-Stokes equations. *Math. Comput.* 22, 745-762.
20. Coyajee, E., Boersma, B.J., (2009). Numerical simulation of drop impact on a liquidliquid interface with a multiple marker front-capturing method. *Journal of Computational Physics* 228 (12), 4444-4467.
21. Darmana, D., Deen, N. G., Kuipers, J. A. M. (2006). Detailed 3D modeling of mass transfer processes in two-phase flows with dynamic interfaces, *Chemical Engineering & Technology* 29(9), 1027-1033.
22. Davidson, M.R., Rudman, M. (2002). Volume-of-fluid calculation of heat or mass transfer across deforming interfaces in two-fluid flow. *Numerical Heat Transfer, Part B: Fundamentals* 41, 291-308.
23. Esmaeeli, A., Tryggvason, G. (1999). Direct numerical simulations of bubbly flows Part 2. Moderate Reynolds number arrays, *J. Fluid Mech.* 385, 325-358.

ICCS Camera Ready Version 2022
To cite this paper please use the final published version:
DOI: 10.1007/978-3-031-08760-8_24

24. Gaskell, P.H. and Lau, A.K.C., (1988). Curvature-compensated convective transport: SMART a new boundedness-preserving transport algorithm, *Int. J. Numer. Methods* 8, 617-641.
25. Gottlieb, S., Shu, C.W. (1998). Total Variation Dimishing Runge-Kutta Schemes, *Mathematics of Computations* 67, 73-85.
26. Gutiérrez, E., Balcázar, N., Bartrons, E., Rigola, J. (2017). Numerical study of Taylor bubbles rising in a stagnant liquid using a level-set/moving-mesh method. *Chemical Engineering Science* 164. 102-117.
27. Hirt, C., Nichols, B. (1981). Volume of fluid (VOF) method for the dynamics of free boundary, *J. Comput. Phys.* 39, 201-225
28. Ishii, M., Hibiki, T., Thermo-Fluid Dynamics of Two-Phase Flow. 2nd edition, Springer, New-York, 2010.
29. Jasak, H. and Weller, H. G. (2000). Application of the finite volume method and unstructured meshes to linear elasticity, *Int. J. Numer. Meth. Engng.* 48, 267-287.
30. Koynov, A., Khinast, J. G., Tryggvason, G. (2005). Mass transfer and chemical reactions in bubble swarms with dynamic interfaces, *AIChE Journal* 51(10), 2786-2800.
31. Lochiel, A.,Calderbank,P. 1964. Mass transfer in the continuous phase around axisymmetric bodies of revolution. *Chem.Eng.Sci.* 19, 471-484.
32. Mavriplis, D. J., 2007. Unstructured Mesh Discretizations and Solvers for Computational Aerodynamics. *18th Computational Fluid Dynamics Conference*, AIAA Paper 2007-3955, Miami, FL, doi:10.2514/6.2007-3955.
33. Olsson, E., Kreiss, G. (2005). A conservative level set method for two phase flow, *J. Comput. Phys.* 210, 225-246.
34. Osher, S., Sethian, J.A. (1988). Fronts propagating with curvature-dependent speed: Algorithms based on Hamilton-Jacobi formulations, *J. Comput. Phys.* 79, 175-210.
35. Rhie, C.M., Chow, W.L. (1983). Numerical Study of the Turbulent Flow past an Airfoil with Trailing Edge Separation, *AIAA J.* 21, 1525-1532.
36. Roghair, I., Van Sint Annaland, M., Kuipers, J.A.M. (2016). An improved Front-Tracking technique for the simulation of mass transfer in dense bubbly flows. *Chem. Eng. Sci.* 152, 351-369.
37. Sussman, M., Smereka, P., Osher, S. (1994). A Level Set Approach for Computing Solutions to Incompressible Two-Phase Flow, *J. Comput. Phys.* 144, 146-159.
38. Sussman, M., Puckett, E.G., 2000. A Coupled Level Set and Volume-of-Fluid Method for Computing 3D and Axisymmetric Incompressible Two-Phase Flows, J. Comput. Phys. 162, 301-337.
39. Sun, D.L., Tao, J., W.Q., 2010. A coupled volume-of-fluid and level-set (VOSET) method for computing incompressible two-phase flows, International Journal of Heat and Mass Transfer 53, 645-655.
40. Sweby, P.K., 1984. High Resolution Using Flux Limiters for Hyperbolic Conservation Laws, SIAM Journal on Numerical Analysis 21, 995-1011.
41. Tryggvason, G., Bunner, B., Esmaeeli, A., Juric, D., Al-Rawahi, N., Tauber, W., Han, J., Nas, S., Jan, Y-J. (2001). A Front-Tracking Method for the Computations of Multiphase Flow, *J. Comput. Phys.* 169, 708-759.
42. Winnikow, S., 1967. Letter to the Editors. Chem. Eng. Sci. 22 (3), 477.

ICCS Camera Ready Version 2022
To cite this paper please use the final published version:
DOI: 10.1007/978-3-031-08760-8_24